Chemical Science

EDGE ARTICLE

View Article Online
View Journal | View Issue

Cite this: *Chem. Sci.*, 2019, **10**, 8768

All publication charges for this article have been paid for by the Royal Society of Chemistry

Photoefficient 2nd generation molecular motors responsive to visible light†

Lukas Pfeifer, Maximilian Scherübl, Maximilian Fellert, Wojciech Danowski, Jinling Cheng, Jasper Pol and Ben L. Feringa *

Received 2nd May 2019
Accepted 31st July 2019

DOI: 10.1039/c9sc02150g

rsc.li/chemical-science

Molecular motors that operate with high efficiency using visible light are attractive for numerous applications. Here the synthesis and characterisation of three novel visible light switchable 2nd generation molecular motors is presented. Two of them are based on push–pull systems with the third one possessing an extended π-system. With a maximum effective excitation wavelength of 530 nm we designed the most red-shifted artificial rotary motor known to date. All three motors benefit from efficient switching to the metastable isomer, high quantum yields and excellent photostability setting them apart from visible light switchable motors reported previously. The activation barriers of the rate-determining thermal helix inversion could be accurately predicted using DFT calculations and differences between the motors can be explained by distinct transition state structures. Enantiomers of push–pull motors were successfully separated and their helical twisting power in E7 liquid crystals was determined.

Introduction

With the focus in chemistry gradually shifting from the synthesis of structure to the synthesis of function,[1] interest in dynamic systems like artificial molecular motors has increased sharply over the last two decades.[2–12] New designs for rotary molecular motors have been introduced[13,14] and various ways to control their speed of rotation described.[15–21] Moreover, this class of molecular motors has been used to exert spatio-temporal control over properties of materials[22–24] and, most recently, our group described assembly into an artificial muscle-type actuator responsive to light and heat.[25]

However, these applications depend on the use of high-energy UV-light to drive the rotation of the employed motors, limiting their potential, especially with regard to use in soft materials and biological settings. Recently, efforts have been made to drive motor rotation using benign visible light by either using triplet–triplet energy transfer from an attached dye as an alternative mechanisms of excitation,[26] complexation of Ru^{II} to a bipyridine derived motor[17] or red-shifting the absorption of the molecular motor core. The latter has been achieved by introduction of electron-donating and -withdrawing substituents to create an electronic push–pull system across the stator (Fig. 1A)[27] or enlarging the π-system of the stator (Fig. 1B).[28] However, both systems suffer from drawbacks in the form of a modest red-shift and low quantum yields, respectively. In 2015, Dube and co-workers described a novel hemithioindigo motor responsive up to 505 nm (*E*-isomer, Fig. 1C).[29–31] A related photon-only molecular motor was disclosed in 2018.[32]

However, in view of future applications it is evident that there is a major need for distinct rotary motors which are able to perform full 360° rotations using low-energy light. We further explored the use of push–pull systems to achieve enhanced red-shifting of the absorption maximum by installing substituents in the stator and rotor halves, in conjugation with the central double-bond serving as the axle of the motor (Fig. 1D). This design was expected to have a significantly greater impact than

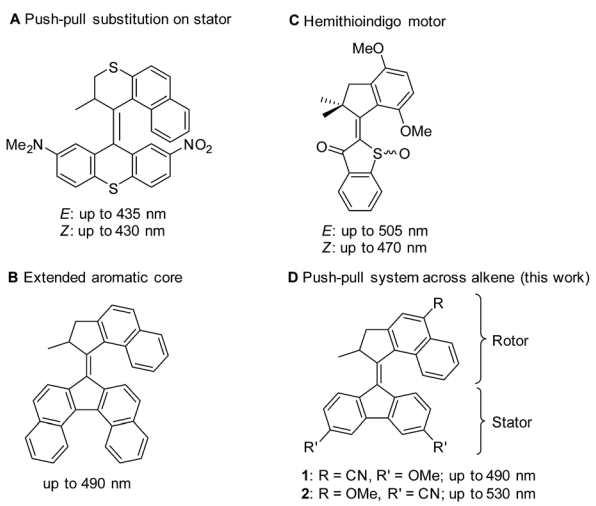

Fig. 1 Summary of approaches for the preparation of molecular motors with red-shifted absorption maxima. Wavelengths refer to the low-energy onsets of absorption.

Stratingh Institute for Chemistry, University of Groningen, Nijenborgh 4, 9747 AG Groningen, The Netherlands. E-mail: b.l.feringa@rug.nl

† Electronic supplementary information (ESI) available. See DOI: 10.1039/c9sc02150g

the previous attempts (Fig. 1A and B) of manipulating the electronic structure of a classic 2nd generation molecular motor.

Here the synthesis and properties of three novel motors efficiently driven by visible light as well as their properties as dopants for liquid crystals are presented.

Results and discussion

Initial TD-DFT (CAM-B3LYP, 6-311G++(d,p)) calculations in Gaussian 16[33] showed a significant effect on the absorption maximum (λ_{max}), when placing CN-groups conjugated to the central alkene on the rotor or stator of a 2nd generation molecular motor. This was further increased upon introducing OMe substituents in the respective other half, thereby creating the desired push–pull effect across the alkene axle. The compounds had a predicted HOMO–LUMO gap corresponding to light of a wavelength >410 nm, a significant increase compared to the unsubstituted parent compound (Fig. 2).[18] The electron density distributions in the Frontier orbitals, furthermore, closely resemble those of the parent motor with HOMO and LUMO being bonding and antibonding, respectively, regarding the central alkene, indicating that single-electron photoexcitation should lead to the desired *E*/*Z*-isomerization.[28]

OMe substituents were chosen as they can serve as handles for subsequent introduction of more complex substituents, granting the motors additional properties (*e.g.* surface attachment, metal binding). They have also previously been shown to be compatible with the conditions during synthesis of molecular motors and to not interfere with the desired mechanical properties.

Synthesis

A general synthetic route including initial preparation of Br- and OMe-substituted stator and rotor halves, subsequent formation of the overcrowded alkene *via* diazo-thioketone coupling (Barton–Kellogg) and final Pd-catalysed cyanation was designed (Scheme 1).

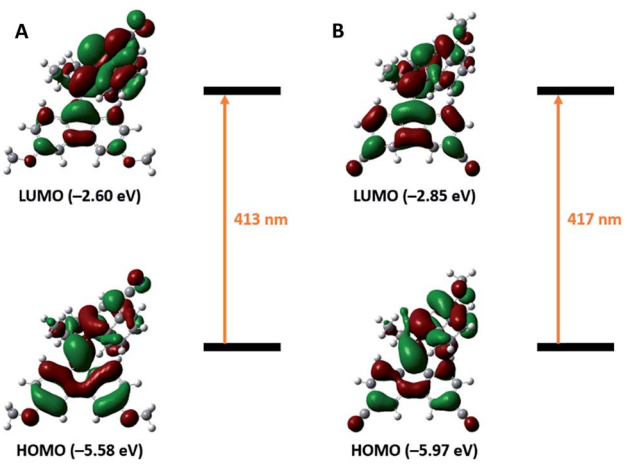

Fig. 2 Structures and calculated (TD-DFT, CAM-B3LYP, 6-311G++(d,p)) Frontier orbitals of 2nd generation molecular motors $\mathbf{1_s}$ (A) and $\mathbf{2_s}$ (B).

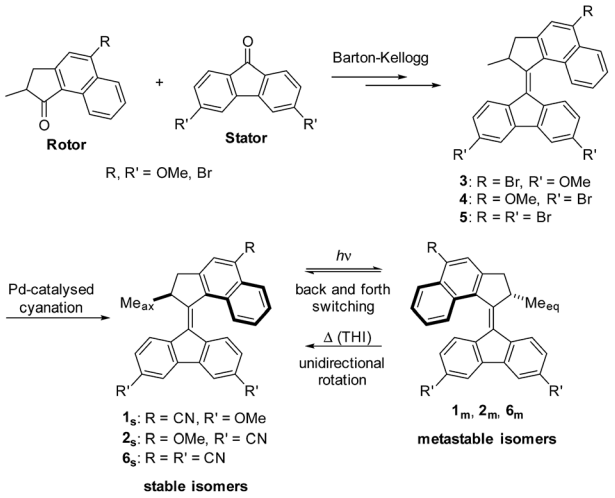

Scheme 1 General synthetic route to CN-substituted 2nd generation molecular motors and pathways for switching as well as unidirectional rotation.

In addition to the two push–pull motors $\mathbf{1_s}$ and $\mathbf{2_s}$ tri-cyano-substituted motor $\mathbf{6_s}$ was prepared, in order to compare the effects of push–pull substitution to the extension of the π-system by the CN-groups in $\mathbf{6_s}$.

Following the general route outlined above, motors $\mathbf{1_s}$, $\mathbf{2_s}$ and $\mathbf{6_s}$ were obtained in 7, 5 and 5 linear steps from commercial compounds in overall yields of 3–10%. Final compounds were characterised by NMR and MS (see ESI† for details).

UV-vis absorption spectra

Initial UV-vis studies on novel motors $\mathbf{1_s}$, $\mathbf{2_s}$ and $\mathbf{6_s}$ revealed absorption maxima (λ_{max}) between 421–453 nm for the respective HOMO–LUMO transitions (Fig. 3). Introduction of three CN-group in $\mathbf{6_s}$ (λ_{max} = 421 nm) led to a redshift comparable to push–pull motor $\mathbf{1_s}$ (λ_{max} = 422 nm), whereas λ_{max} of $\mathbf{2_s}$ was further red-shifted to 453 nm. This constitutes a redshift of >60 nm compared to the parent compound.[18] The HOMO–LUMO band also tails further towards the red part of the visible spectrum, with the onset being red-shifted by >80 nm compared to the unsubstituted motor. Irradiation with 420 nm ($\mathbf{1_s}$, $\mathbf{6_s}$) and 455 nm ($\mathbf{2_s}$) light, respectively, led to the appearance of new red-shifted bands, characteristic for the formation of the metastable isomers of fluorene-based 2nd generation molecular motors.[18,21] Clean isosbestic points were observed for all three compounds during irradiation to the corresponding photo-stationary states (PSS) and subsequent thermal helix inversion (THI) (Fig. S6†), confirming a selective transition between stable and metastable isomers with lifetimes of involved photo-excited states being negligibly short under these conditions.[34,35]

Characterisation of rotations by ^{1}H NMR

The ratios of metastable : stable isomers at PSS were established by ^{1}H NMR with *in situ* irradiation, whereby characteristic shifts of signals H_a, H_b and H_c were observed upon formation of metastable isomers (Fig. 4 and S12–16†).

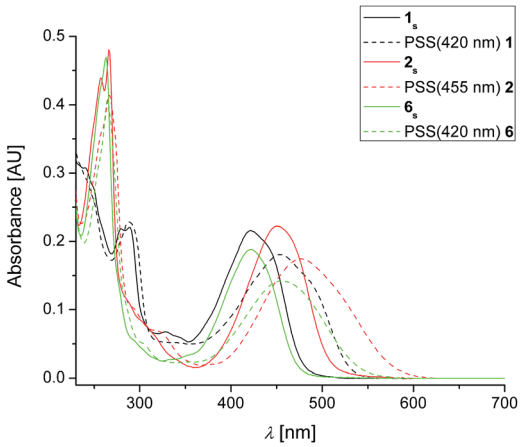

Fig. 3 Plain: UV-vis spectra of $\mathbf{1_s}$, $\mathbf{2_s}$ and $\mathbf{6_s}$ in DCM ($c = 1.0 \times 10^{-5}$ M, $T = -10$ °C). Dashed: UV-vis spectra after irradiation to PSS with 420 nm ($\mathbf{1_s}$, $\mathbf{6_s}$) and 455 nm ($\mathbf{2_s}$) light, respectively.

Table 1 provides an overview of the ratios of metastable : stable isomers for motors **1**, **2** and **6** at PSS using LEDs with different emission maxima for excitation (see ESI† for details on LEDs). It is evident that motors **1** and **6** can be driven with light up to 490 nm whereas $\mathbf{2_s}$ remains responsive up to 530 nm, the highest value reported to date for an artificial rotary molecular motor operated by direct absorption of incident light.

Both motors **1** and **2** show comparable ratios of metastable : stable isomers at PSS, when irradiated close to their respective $\lambda_{max,s}$ (420 nm for $\mathbf{1_s}$, 455 nm for $\mathbf{2_s}$). Given the considerable difference between the ratios of molar absorption coefficients (ε) of stable and metastable isomers of the two motors at these wavelengths (Table S8†), this also suggests

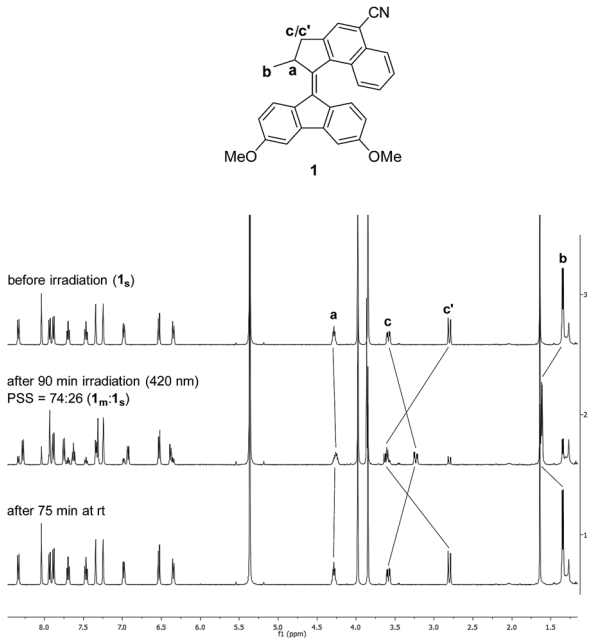

Fig. 4 ^{1}H NMR spectra of **1** in DCM-d_2 ($c = 5.0 \times 10^{-3}$ M, $T = -10$ °C) before irradiation ($\mathbf{1_s}$), at PSS and after completed THI.

Table 1 Ratios of metastable : stable isomers of motors **1**, **2** and **6** at different excitation wavelengths (λ_{exc}) as measured by ^{1}H NMR in DCM-d_2 ($c = 5.0 \times 10^{-3}$ M, $T = -10$ °C, $t_{irr} = 90$ min)

λ_{exc} [nm]	Motor	PSS [m : s]
420	**1**	74 : 26
	6	88 : 12
455	**1**	50 : 50
	2	76 : 24
	6	63 : 37
470	**1**	25 : 75
	2	63 : 37
	6	34 : 66
490	**1**	<5 : >95
	2	32 : 68
	6	<5 : >95
505	**2**	24 : 76
530	**2**	<5 : >95

a difference in the ratios of quantum yields for the photochemical forward (stable → metastable) and back-reactions (metastable → stable) (*vide infra*). By contrast, a significantly higher proportion of metastable isomer of 88% is formed upon irradiation of a sample of $\mathbf{6_s}$ with 420 nm light. This represents the highest PSS ratio obtained for a 2nd generation molecular motor with a central alkene flanked by two five-membered rings. The higher ratio of ε of stable and metastable isomers of **6** at 420 nm (2.21) compared to motors **1** and **2** at 420 nm (2.05) and 455 nm (1.70), respectively, is one of the factors contributing to this property. Generally, at longer wavelengths the ratios of metastable : stable isomers significantly favour the latter due to the increasing difference in ε.

Eyring analysis

Whereas determination of ratios of isomers at PSS provides valuable information regarding the efficiency with which a molecular motor can be operated and its potential utility as a two-state switch, another one of its central properties, speed of rotation, depends on the activation barrier of the rate-determining THI. Eyring analysis was therefore performed to determine the Gibbs energy of activation ($\Delta^{\ddagger}G^{\circ}_{exp}$) for THI of $\mathbf{1_m}$, $\mathbf{2_m}$ and $\mathbf{6_m}$ at 20 °C from which the thermal half-life ($t^{\circ}_{1/2}$) of these metastable isomers could be calculated (Table 2).

Although experimental Gibbs energies are within 5 kJ mol^{-1} of each other their values could be accurately reproduced by DFT calculation ($\Delta^{\ddagger}G^{\circ}_{calc}$) allowing for rationalisation of the observed differences by comparing the optimised structures of the respective metastable isomers and THI transition states (see ESI†). The calculated geometries for the metastable isomers of all three motors are nearly identical (RMS deviations: 0.002–0.004, Table S4†),[36,37] suggesting the differences to arise from deviations in the TS structures. Indeed, the largest elongation of the central alkene upon formation of TS from metastable

isomer is required for **2** followed by **6** and **1** mirroring the trend of $\Delta^{\ddagger}G^{\circ}$. For motor 1 this can be explained with the observed bending of the OMe-substituted fluorene stator in the TS making it easier for the two halves to slip past each other. In the case of $\mathbf{2_{TS}}$ and $\mathbf{6_{TS}}$, however, the stator preserves its flat geometry, maintaining maximum overlap of π-orbitals instead.

With the geometries of the motor cores of $\mathbf{2_{TS}}$ and $\mathbf{6_{TS}}$ overlapping almost perfectly (RMS deviation: 0.01, Table S3†) the observed difference in $\Delta^{\ddagger}G^{\circ}$ is most likely due to electronic effects as the push–pull substitution pattern facilitates the build-up of partial charges in the stator and rotor halves of $\mathbf{2_m}$ (see Table S6†), which might contribute to its stability. This is in line with $\mathbf{2_m}$ being more stabilized than $\mathbf{2_{TS}}$ compared to the corresponding structures of motor **6** taking the energy difference between the stable isomers as reference (Table S1†).

Quantum yields

The effects of introducing a push–pull regime across the central alkene on the photoefficiency of these motors was investigated by determining the quantum yields for photoisomerization (φ) close to their respective $\lambda_{max,s}$ (420 nm for **1**, 455 nm for **2**). The quantum yields were measured under steady-state conditions compared to decomposition of ferrioxalate as standard (see ESI†). As can be seen in Table 3, motors **1** and **2** exhibit quantum yields for the forward reaction, $\varphi_{s\rightarrow m}$, of 11.5 ± 0.2% and 5.84 ± 0.27%, respectively. These are among the highest quantum yields of any artificial rotary molecular motor measured to date and are comparable to a series of related, monosubstituted motors, suggesting that push–pull substitution does not negatively impact photoefficiency.[2,35]

Quantum yields for the back-reaction, $\varphi_{m\rightarrow s}$, were calculated to be 7.85 ± 0.17% and 3.13 ± 0.14%, respectively, and therefore significantly lower than those for the forward reaction, in accordance with the excess of metastable isomers at PSS upon irradiation with 420 nm (for **1**) and 455 nm (for **2**), respectively. Motor **2** displays a higher ratio of $\varphi_{s\rightarrow m} : \varphi_{m\rightarrow s}$, which helps to explain the almost identical excess of metastable isomer at PSS for **1** (irradiation with 420 nm) and **2** (irradiation with 455 nm) in spite of a larger molar absorption coefficient of $\mathbf{2_m}$ relative to $\mathbf{2_s}$ at $\lambda_{max,s}$ compared to motor **1**. Interestingly, the quantum yields for the back-reaction in the aforementioned series of structurally related motors had previously been found to be higher than that of the forward reaction.[35] Although this might be an effect of the push–pull substitution pattern of **1** and **2**, $\varphi_{s\rightarrow m}$ and $\varphi_{m\rightarrow s}$ for **6** at 420 nm were found to be 4.93 ± 0.05% and 1.48 ± 0.02%, respectively, showing that this reversal in photoefficiency can also be achieved by installing three CN-groups in conjugation with the central alkene. Compound **6** therefore also possesses the highest ratio of $\varphi_{s\rightarrow m} : \varphi_{m\rightarrow s}$ which, together with the significantly higher molar absorption coefficient of $\mathbf{6_s}$ at $\lambda_{max,s}$ compared to $\mathbf{6_m}$ (*vide supra*), helps to explain the high PSS ratio compared to structurally related motors. The measured quantum yields for the forward reaction, especially in the case of **1**, also compare favourably to the maximum quantum yield of *ca.* 20–30% calculated for the photochemical *E*/*Z* isomerisation of overcrowded alkenes by non-adiabatic molecular dynamics simulations.[38]

Table 3 Quantum yields for the forward ($\varphi_{s\rightarrow m}$) and back-reaction ($\varphi_{m\rightarrow s}$) of motors **1**, **2** and **6**

Motor	$\varphi_{s\rightarrow m}$ [%]	$\varphi_{m\rightarrow s}$ [%]
1	11.5 ± 0.2	7.85 ± 0.17
2	5.84 ± 0.27	3.13 ± 0.14
6	4.93 ± 0.05	1.48 ± 0.02

Fatigue studies

As stated before, the main reasons for red-shifting the absorption spectrum of artificial molecular motors are the advantages visible light provides over UV light regarding applications in biology and materials science. However, in order for compounds to be suitable for these applications it is necessary for them to show excellent (photo)stability to avoid premature fatigue. Therefore, solutions of $\mathbf{1_s}$, $\mathbf{2_s}$ and $\mathbf{6_s}$ in DCM were irradiated to PSS ten times using LEDs of 420 nm ($\mathbf{1_s}$, $\mathbf{6_s}$) and 455 nm ($\mathbf{2_s}$), respectively. After each irradiation as well as subsequent THI UV-vis absorption spectra were recorded. Fig. 5 and S11 display plots of the absorbances measured at 420 nm ($\mathbf{1_s}$, $\mathbf{6_s}$) and 455 nm ($\mathbf{2_s}$), respectively.

This revealed the three novel motors to possess outstanding (photo)stability under these conditions, as no significant change in absorption was found during these studies, making them promising candidates for the development of novel light and heat responsive materials.

Use as liquid crystal dopants

In 2002, our group for the first time reported the use of enantiomerically pure artificial rotary molecular motors as chiral dopants to obtain photo-responsive cholesteric liquid crystals, demonstrating their ability to alter the reflected wavelength upon generation of the metastable isomer *in situ* in the liquid crystal material.[39] However, the UV light used in the original as well as follow-up studies remains one of the major limitations

Table 2 Summary of thermodynamic parameters for THI of $\mathbf{1_m}$, $\mathbf{2_m}$ and $\mathbf{6_m}$ as determined by Eyring analysis as well as calculated Gibbs energies of activation (GS-DFT, B3LYP, 6-311++G(d,p))

	$\Delta H^{\ddagger}$ [kJ mol^{-1}]	$\Delta S^{\ddagger}$ [J K^{-1} mol^{-1}]	$\Delta^{\ddagger}G^{\circ}_{exp}$ [kJ mol^{-1}]	$\Delta^{\ddagger}G^{\circ}_{calc}$ [kJ mol^{-1}]	$t^{\circ}_{1/2}$ [s]
$\mathbf{1_m}$	76.6 ± 0.8	−32.6 ± 3.0	86.2 ± 0.1	86.1	258 ± 7
$\mathbf{2_m}$	83.1 ± 0.9	−27.2 ± 3.1	91.0 ± 0.1	90.9	1900 ± 21
$\mathbf{6_m}$	83.1 ± 0.9	−21.3 ± 3.2	89.3 ± 0.1	89.1	934 ± 15

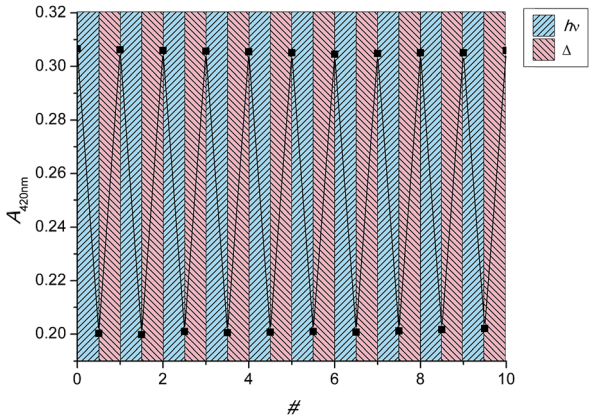

Fig. 5 Fatigue study on motor **1**. Conditions: DCM, 1.0×10^{-5} M, 25 °C, 420 nm LED.

Table 4 Helical twisting powers (β) of enantiomerically pure stable isomers as well as PSS mixtures of motors **1** (λ_{exc} = 420 nm) and **2** (λ_{exc} = 455 nm) used as dopants (*ca.* 1 wt%) in E7 liquid crystals

	1	**2**
β_s ((*P*)-(*R*)/(*M*)-(*S*)) [μm^{-1}]	12/−12	9/−9
β_{PSS} ((*P*)-(*R*)/(*M*)-(*S*)) [μm^{-1}]	−10/10	−6/6
$\Delta\beta$ ((*P*)-(*R*)/(*M*)-(*S*)) [μm^{-1}]	22/−22	15/−15

of this technology.[24,40–42] For this reason, we decided to study the efficacy of our novel visible light responsive push–pull motors $\mathbf{1_s}$ and $\mathbf{2_s}$ as switchable chiral dopants to obtain cholesteric E7 liquid crystals. Table 4 gives an overview of the measured helical twisting powers (β) for enantiomerically pure stable isomers and PSS mixtures of motors **1** (λ_{exc} = 420 nm) and **2** (λ_{exc} = 455 nm).

The obtained values of ±12 μm^{-1} and ±9 μm^{-1} for $\mathbf{1_s}$ and $\mathbf{2_s}$ as well as ±10 μm^{-1} and ±6 μm^{-1} for the corresponding PSS mixtures, respectively, are lower than those of the unsubstituted parent motor.[43] However, as reversal of the sign of the cholesteric helicity is found in the PSS mixtures compared to the stable isomers, values for $\Delta\beta$ of ±22 and ±15 were obtained upon photoswitching. This inversion of sign also indicates that it is helical chirality and not point chirality that dominates the induction of the pitch of E7 liquid crystals. However, with DFT structures of both stable and metastable isomers of motors **1** and **2** overlapping almost perfectly (see ESI†) it seems that in this case the strength of interaction between liquid crystal and dopant rather than a dopant's more or less pronounced helical structure is crucial for achieving high values for β. This is supported by the fact that, in the case of these motors, molar ellipticities (θ_M) at characteristic wavelengths are of similar magnitude (see ESI†) and show no clear trend or correlation with β, as far as we know. This study also represents the first time visible light switchable motors have been successfully employed to alter the pitch of a cholesteric E7 liquid crystal.

Conclusions

We have demonstrated that the use of push–pull systems holds great potential for the development of a range of tailor-made light-driven molecular motors for specific applications. With the present design we have successfully overcome the need for high energy UV light to power artificial rotary systems, while keeping with the versatile design of 2nd generation molecular motors and without employing additional dyes or sensitizers. Most remarkably, $\mathbf{2_s}$ is responsive to light up to 530 nm, an unprecedented redshift for an artificial rotary molecular motor. In the case of motor **6**, the high ratio of metastable : stable isomers at PSS, especially at $\lambda_{max,s}$, demonstrates the possibility to tune this parameter by judicious choice of substituents. The straightforward synthesis as well as high quantum yields and excellent (photo)stability of these compounds make them promising targets for further investigation and application in smart materials.

Conflicts of interest

The authors declare there to be no conflicts of interest.

Acknowledgements

Financial support from The Netherlands Organization for Scientific Research (NWO-CW), the Netherlands Foundation for Fundamental Research on Matter (FOM, a subsidiary of NWO), The Royal Netherlands Academy of Arts and Sciences (KNAW), the European Research Council (Advanced Investigator Grant No. 694345 to BLF), the European Commission (MSCA-IF No. 793082 to LP, Erasmus + scholarships to MS and MF), the Dutch Ministry of Education, Culture and Science (Gravitation Program 024.001.035), the Cusanuswerk (German Episcopal Scholarship Foundation), and the University of Groningen is gratefully acknowledged.

Notes and references

1 D. Sluysmans and J. F. Stoddart, *Proc. Natl. Acad. Sci. U. S. A.*, 2018, **115**, 9359–9361.
2 D. Roke, S. J. Wezenberg and B. L. Feringa, *Proc. Natl. Acad. Sci. U. S. A.*, 2018, **115**, 9423–9431.
3 S. Kassem, T. van Leeuwen, A. S. Lubbe, M. R. Wilson, B. L. Feringa and D. A. Leigh, *Chem. Soc. Rev.*, 2017, **46**, 2592–2621.
4 C. J. Bruns and J. F. Stoddart, *The Nature of the Mechanical Bond*, John Wiley & Sons, Inc., Hoboken, NJ, USA, 2016.
5 S. Erbas-Cakmak, D. A. Leigh, C. T. McTernan and A. L. Nussbaumer, *Chem. Rev.*, 2015, **115**, 10081–10206.
6 E. Moulin, G. Cormos and N. Giuseppone, *Chem. Soc. Rev.*, 2012, **41**, 1031–1049.
7 C. Pezzato, C. Cheng, J. F. Stoddart and R. D. Astumian, *Chem. Soc. Rev.*, 2017, **46**, 5491–5507.
8 A. Coskun, M. Banaszak, R. D. Astumian, J. F. Stoddart and B. A. Grzybowski, *Chem. Soc. Rev.*, 2012, **41**, 19–30.

9 P. Ceroni, A. Credi and M. Venturi, *Chem. Soc. Rev.*, 2014, **43**, 4068–4083.
10 K. Kinbara and T. Aida, *Chem. Rev.*, 2005, **105**, 1377–1400.
11 V. Balzani, A. Credi and M. Venturi, *Molecular Devices and Machines: Concepts and Perspectives for the Nanoworld*, Wiley-VCH Verlag GmbH & Co. KGaA, Weinheim, Germany, 2008.
12 *From Non-Covalent Assemblies to Molecular Machines*, ed. J.-P. Sauvage and P. Gaspard, Wiley-VCH Verlag GmbH & Co. KGaA, Weinheim, Germany, 2010.
13 J. C. M. Kistemaker, P. Štacko, D. Roke, A. T. Wolters, G. H. Heideman, M.-C. Chang, P. van der Meulen, J. Visser, E. Otten and B. L. Feringa, *J. Am. Chem. Soc.*, 2017, **139**, 9650–9661.
14 L. Greb and J.-M. Lehn, *J. Am. Chem. Soc.*, 2014, **136**, 13114–13117.
15 A. Faulkner, T. van Leeuwen, B. L. Feringa and S. J. Wezenberg, *J. Am. Chem. Soc.*, 2016, **138**, 13597–13603.
16 R. Dorel, C. Miró, Y. Wei, S. J. Wezenberg and B. L. Feringa, *Org. Lett.*, 2018, **20**, 3715–3718.
17 S. J. Wezenberg, K.-Y. Chen and B. L. Feringa, *Angew. Chem., Int. Ed.*, 2015, **54**, 11457–11461.
18 J. Vicario, A. Meetsma and B. L. Feringa, *Chem. Commun.*, 2005, 5910–5912.
19 T. Fernández Landaluce, G. London, M. M. Pollard, P. Rudolf and B. L. Feringa, *J. Org. Chem.*, 2010, **75**, 5323–5325.
20 M. M. Pollard, A. Meetsma and B. L. Feringa, *Org. Biomol. Chem.*, 2008, **6**, 507–512.
21 J. Vicario, M. Walko, A. Meetsma and B. L. Feringa, *J. Am. Chem. Soc.*, 2006, **128**, 5127–5135.
22 Q. Li, G. Fuks, E. Moulin, M. Maaloum, M. Rawiso, I. Kulic, J. T. Foy and N. Giuseppone, *Nat. Nanotechnol.*, 2015, **10**, 161–165.
23 J. T. Foy, Q. Li, A. Goujon, J.-R. Colard-Itté, G. Fuks, E. Moulin, O. Schiffmann, D. Dattler, D. P. Funeriu and N. Giuseppone, *Nat. Nanotechnol.*, 2017, **12**, 540–545.
24 R. Eelkema, M. M. Pollard, J. Vicario, N. Katsonis, B. S. Ramon, C. W. M. Bastiaansen, D. J. Broer and B. L. Feringa, *Nature*, 2006, **440**, 163.
25 J. Chen, F. K.-C. Leung, M. C. A. Stuart, T. Kajitani, T. Fukushima, E. van der Giessen and B. L. Feringa, *Nat. Chem.*, 2017, **10**, 132–138.
26 A. Cnossen, L. Hou, M. M. Pollard, P. V. Wesenhagen, W. R. Browne and B. L. Feringa, *J. Am. Chem. Soc.*, 2012, **134**, 17613–17619.
27 R. A. van Delden, N. Koumura, A. Schoevaars, A. Meetsma and B. L. Feringa, *Org. Biomol. Chem.*, 2003, **1**, 33–35.
28 T. van Leeuwen, J. Pol, D. Roke, S. J. Wezenberg and B. L. Feringa, *Org. Lett.*, 2017, **19**, 1402–1405.
29 M. Guentner, M. Schildhauer, S. Thumser, P. Mayer, D. Stephenson, P. J. Mayer and H. Dube, *Nat. Commun.*, 2015, **6**, 8406.
30 L. A. Huber, K. Hoffmann, S. Thumser, N. Böcher, P. Mayer and H. Dube, *Angew. Chem., Int. Ed.*, 2017, **56**, 14536–14539.
31 R. Wilcken, M. Schildhauer, F. Rott, L. A. Huber, M. Guentner, S. Thumser, K. Hoffmann, S. Oesterling, R. de Vivie-Riedle, E. Riedle and H. Dube, *J. Am. Chem. Soc.*, 2018, **140**, 5311–5318.
32 A. Gerwien, P. Mayer and H. Dube, *J. Am. Chem. Soc.*, 2018, **140**, 16442–16445.
33 M. J. Frisch, G. W. Trucks, H. B. Schlegel, G. E. Scuseria, M. A. Robb, J. R. Cheeseman, G. Scalmani, V. Barone, G. A. Petersson, H. Nakatsuji, X. Li, M. Caricato, A. V. Marenich, J. Bloino, B. G. Janesko, R. Gomperts, B. Mennucci, H. P. Hratchian, J. V. Ortiz, A. F. Izmaylov, J. L. Sonnenberg, D. Williams-Young, F. Ding, F. Lipparini, F. Egidi, J. Goings, B. Peng, A. Petrone, T. Henderson, D. Ranasinghe, V. G. Zakrzewski, J. Gao, N. Rega, G. Zheng, W. Liang, M. Hada, M. Ehara, K. Toyota, R. Fukuda, J. Hasegawa, M. Ishida, T. Nakajima, Y. Honda, O. Kitao, H. Nakai, T. Vreven, K. Throssell, J. A. Montgomery Jr., J. E. Peralta, F. Ogliaro, M. J. Bearpark, J. J. Heyd, E. N. Brothers, K. N. Kudin, V. N. Staroverov, T. A. Keith, R. Kobayashi, J. Normand, K. Raghavachari, A. P. Rendell, J. C. Burant, S. S. Iyengar, J. Tomasi, M. Cossi, J. M. Millam, M. Klene, C. Adamo, R. Cammi, J. W. Ochterski, R. L. Martin, K. Morokuma, O. Farkas, J. B. Foresman and D. J. Fox, *Gaussian 16, Revision B.01*, Gaussian Inc., Wallingford CT, 2016.
34 J. Conyard, K. Addison, I. A. Heisler, A. Cnossen, W. R. Browne, B. L. Feringa and S. R. Meech, *Nat. Chem.*, 2012, **4**, 547–551.
35 J. Conyard, A. Cnossen, W. R. Browne, B. L. Feringa and S. R. Meech, *J. Am. Chem. Soc.*, 2014, **136**, 9692–9700.
36 H. J. C. Berendsen, D. van der Spoel and R. van Drunen, *Comput. Phys. Commun.*, 1995, **91**, 43–56.
37 E. Lindahl, B. Hess and D. van der Spoel, *J. Mol. Model.*, 2001, **7**, 306–317.
38 A. Kazaryan, Z. Lan, L. V. Schäfer, W. Thiel and M. Filatov, *J. Chem. Theory Comput.*, 2011, **7**, 2189–2199.
39 R. A. van Delden, N. Koumura, N. Harada and B. L. Feringa, *Proc. Natl. Acad. Sci. U. S. A.*, 2002, **99**, 4945–4949.
40 D. Pijper, M. G. M. Jongejan, A. Meetsma and B. L. Feringa, *J. Am. Chem. Soc.*, 2008, **130**, 4541–4552.
41 T. Orlova, F. Lancia, C. Loussert, S. Iamsaard, N. Katsonis and E. Brasselet, *Nat. Nanotechnol.*, 2018, **13**, 304–308.
42 P. Sleczkowski, Y. Zhou, S. Iamsaard, J. J. de Pablo, N. Katsonis and E. Lacaze, *Proc. Natl. Acad. Sci. U. S. A.*, 2018, **115**, 4334–4339.
43 R. Eelkema, M. M. Pollard, N. Katsonis, J. Vicario, D. J. Broer and B. L. Feringa, *J. Am. Chem. Soc.*, 2006, **128**, 14397–14407.